Analysis of refrigerant flow and deformation for a flexible short-tube using a finite element model

Ramadan Bassiouny[a], Dennis L. O'Neal[b],*

[a]*Department of Mechanical Engineering, Minia University, Minia 61111, Egypt*
[b]*Department of Mechanical Engineering, Texas A&M University, College Station, TX 77843-3123, USA*

Abstract

A finite element model was used to simulate single-phase flow of R-22 through flexible short-tubes. The numerical model included the fluid-structure interaction between the refrigerant and the deformation of the short-tube as upstream pressure was varied. The finite element model was developed using a commercially available finite element package. Short-tubes with moduli of elasticity ranging from 5513 to 9889 kPa were studied. Four upstream and downstream pressures were applied and the upstream subcooling was held at a constant value of 16.7 °C. Mass flow rates from the numerical model were compared to available published experimental results. The study showed that upon deformation the short-tube resembled the shape of a converging-diverging nozzle. Both tube inlet and outlet had a chamfered-like shape after deformation which reduced the pressure drop at the tube inlet. The smaller the modulus of the tube, the larger the chamfered-like angle at the inlet and the higher the pressure drop along the tube due to the higher tube contraction. The results illustrated that as the upstream pressure was increased by 45%, there was almost a 60% decrease in the flow area. The more flexible (5513 kPa) short-tube restricted the mass flow rate more than the most rigid (9889 kPa) short-tube used in this study. The mass flow rates estimated with the finite element model were as much as 14% higher than those from experimental results reported in the literature.
© 2003 Elsevier Ltd and IIR. All rights reserved.

Keywords: Modelling; Flow; Refrigerant; Water; Deformation; Flexible; Flexible tube

Analyse de l'écoulement d'un frigorigène et de la déformation d'un tube flexible par la méthode des éléments finis

1. Introduction

The short-tube is used by United States heat pump manufactures as an expansion device because of its low cost, ease of installation, low maintenance, and high reliability. Short-tubes have either a constant inner diameter flow channel or a tapered channel with a small change in inner diameter from inlet to outlet. Rigid short-tubes are inexpensive and provide adequate flow control in the systems.

A flexible short-tube (Fig. 1) is made of an elasto-meric material that deforms in response to an increased pressure differential across it. The deformation in shape

---

* Corresponding author. Tel.: +1-979-845-5337; fax: +1-979-845-3081.

E-mail address: doneal@mengr.tamu.edu (D.L. O'Neal).

Nomenclature

A	Short-tube cross-sectional (m^2)
C_c	Orifice constant
D	Short-tube diameter (m)
g_{ca}	Dimension gravity constant, 1.296×10^{10} [s^2 N/(h^2 kN)]
L	Short-tube length (m)
L/D	Length over diameter ratio of short-tube
M	Mass flow (kg h^{-1})
P	Pressure (kPa)
SUBC	Subcooling (K)
T	Temperature (K)

Greek symbols

ρ	fluid density (kg m^{-3})

Subscripts

Cr	critical
dn	downstream
ref	reference
sat	saturation
up	upstream

results in a change in flow cross-sectional area as the upstream pressure in the system changes [1–3]. The change in area should provide better flow control of the refrigerant when compared to a conventional rigid short-tube.

A potential advantage of a flexible over a rigid short-tube is that it could provide better flow control by varying its cross-sectional area in response to the pressure change across the compressor. When the condenser pressure increases due to an increase in the ambient temperature above the system design point, a rigid short-tube can sometimes provide a high enough flow rate to flood the compressor with saturated refrigerant. On the other hand, when the condenser pressure

decreases due to a decrease in the ambient temperature, a rigid short-tube passes a lower refrigerant flow rate that can produce high superheat leaving the evaporator. This flow imbalance can affect the system efficiency and performance.

The purpose of this study was to develop a finite element model that could be used to (1) predict the deformation in a flexible short-tube for different moduli of elasticity and system conditions, and (2) estimate the mass flow through the short-tube for R-22. While R-22 is an HCFC and will eventually be phased out from production, the only test data available for a flexible short-tube was with R-22. Thus, the simulation of the short-tube was done with R-22 to help validate the modeling approach. The deformation included a coupled model of the flow field and the structure of the short-tube.

The numerical modeling was limited to single-phase flow conditions because of two reasons. First, the primary purpose of the simulations (as stated in the previous paragraph) was to determine if it was possible to model the change in shape of the short-tube as the upstream pressure increased. Modeling the change in shape of the orifice requires coupling a flow model with a deformation model of the solid. Because the deformation is expected primarily to be dependent on the upstream pressure of the refrigerant and the material selected for the short-tube, the authors felt a single-phase flow model should be sufficient to show how the short-tubes deform with changes in upstream pressure. A second reason for limiting the model to single- phase flow conditions is that there were no reasonably good two-phase finite element models available at the time of this study.

For the short-tube, three moduli of elasticity were evaluated: 5513, 7084 and 9889 kPa. Upstream pressures ranged from 1179 to 2144 kPa. Estimates for the change in shape of the short-tubes as well as refrigerant mass flow are presented. With the mass flow, results were compared to previously published experimental data [4].

2. Previous work

Flow behavior through short-tubes was a major focus of several previous studies [5–11]. These studies dealt primarily with flow behavior, flow metastability, or mass flow-rate modeling for single and two-phase flow of refrigerants. They considered different operating conditions that included inlet subcooling/quality, upstream and downstream pressure, and inlet and exit edge shape.

The sharp edge at the inlet of the short-tube significantly affects the pressure drop through the short-tube, and consequently the mass flow rate. Krakow and
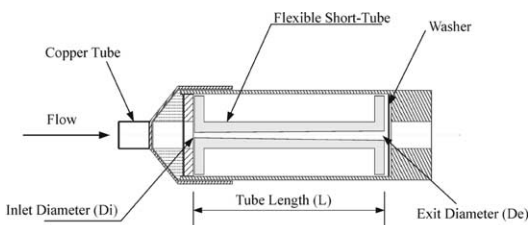

Fig. 1. Schematic of the flexible short-tube orifice test section with downstream washer.

Lin [6] attributed the pressure drop across a fluid element to three effects: specific volume variation, cross-sectional area variation, and viscosity (wall friction). The effect of inlet and exit chamfering was investigated in [7–11]. Aaron and Domanski [7] reported that 45° chamfering at the tube inlet caused a 5–25% increase in the mass flow rate depending on the L/D ratio and chamfering depth. Chamfering at the tube exit had no appreciable effect on the mass flow rate, which was also observed by Kim [9] and Kim and O'Neal [10,11]. Kuehl and Goldschmidt [8] showed that the mass flow rate increased with increasing tube diameter and the flow inlet subcooling.

A semi-empirical correlation to predict the mass flow rate before the flashing point as a function of both the upstream and saturation pressure was developed by Kim and O'Neal [11]. Reducing the downstream pressure caused a corresponding reduction in the downstream temperatures due to the fact that the downstream is saturated [11]. Consequently, the heat transfer along the tube would delay the onset of flashing inside the short-tube. This would tend to increase the mass flow. Reducing the downstream pressure also tended to reduce the average pressure inside the short-tube [7]. Tube diameter was the strongest variable in determining the flow rate [7,9,11]. The mass flow rate was nearly proportional to the square of the short-tube diameter, D [7,9,11]. Empirical correlations were developed that relate mass flow rate, M, to the upstream pressure, P, in the form:

$$M = P^n \qquad (1)$$

where n is a constant dependent on the geometry of the short-tube [7,9].

The only available work on flexible short-tubes was by Kim et al. [4]. The authors experimentally evaluated the overall performance of two flexible short-tubes with two different moduli of elasticity (7084 and 9889 kPa). The tests included a range of operating variables such as inlet subcooling/quality, upstream pressure, and downstream pressure. They observed that the mass flow rate through the flexible short-tubes was strongly dependent on the modulus of elasticity of the material and on upstream pressure. For short-tubes with the same undeformed diameter, they concluded that the lower modulus (more flexible) short-tubes had a smaller refrigerant flow than the higher modulus (less flexible) short-tubes. Their study focused on mass flow. No data were collected or observations made about how the tube deformed as the upstream pressure was increased, nor were data collected on the pressure distribution in the short-tube. Thus, a numerical study may provide some insight into both the deformation and pressure distribution of the short-tube under a variety of upstream and downstream conditions.

A semi-empirical correlation was developed in [4] to predict the mass flow rate, M, through flexible short-tubes before flashing. This correlation was based on the single-phase, single-component orifice equation:

$$M = A_s \sqrt{2 g_{ca} \rho (P_{up} - P_f)} \qquad (2)$$

where,

$$P_f = P_{sat} \left[b_1 + b_2 PRA^{b_3} SUBC^{b_4} + b_5 EVAP^{b_6} \right]$$

$PRA = P_{up}/P_{Cr}$
$SUBC = (T_{sat} - T_{up})/T_{Cr}$
$EVAP = (P_{Cr} - P_{down})/P_{Cr}$
T = absolute temperature (K)
T_{cr} = critical temperature (K)
P_{cr} = critical pressure (bar)
P = absolute pressure (bar)
$b_1, b_2 \ldots b_6$ = regression constants (Table 1)

It can be concluded from the above discussion that the tube diameter is the major geometric influence on mass flow rate through short-tubes. Thus, to estimate mass flow through a flexible short-tube, it is important to be able to estimate the change in diameter as the upstream conditions change. A numerical model that includes interaction between the flow and short-tube may provide insights into how the tube is deforming and how different material properties can be used in the tube to "fine tune" the short-tube for the range in pressures expected in the system application.

3. Numerical model and methodology

Because flexible short-tubes can change shape as the upstream pressure changes, modeling them required a methodology that could predict the shape change under a variety of upstream flow conditions. The primary problem with flexible short-tubes is the need to model the fluid-structure interaction between the refrigerant and short-tube. Due to its ability to handle fluid-structure interaction problems and flexibility in terms of

Table 1
Regression constants for Eq. (2) from Kim et al. [4]

Short-tube modulus	b_1	b_2	b_3	b_4	b_5	b_6
7084 kPa	0.9187	10.4091	−0.05	1.1787	−0.0276	0.9241
9889 kPa	1.0434	7.4048	0.0191	1.0421	−0.1683	−0.7797

having different element shapes, the finite element method (FEM) was used.

One previously published study [12] focused on similar fluid–structure interaction problems for a different application. In this study, the authors derived an approach that considered both variations of stress through the thickness and tangential as well as normal surface traction to predict an elastic tube deformation. In their model, the outer surface of the tube was free of traction, the material was neo-Hooken rubber-like, and there were no effects from the tube ends. They mentioned that the problem of viscous flow inside an elastic tube must take into account both the tangential stress and axial varying internal pressure acting on the inner surface. Further, the pressure varies along any streamline even on the tube wall due to the viscous drag.

The axisymmetric computational domain for the flexible tube model is shown in Fig. 2. A commercially available finite element code [13] was chosen to model the flow through the short-tube. This code had the capability to model the fluid-structure interaction required to estimate the change in shape of the short-tube as upstream pressure changed. The continuity, momentum, energy equations for the fluid-flow side, and the stress–strain relations for the structure side are discussed comprehensively in Ref. [13]. The analysis started with a relatively coarse mesh for a rigid short-tube. The pressure distribution inside the short-tube was then estimated with the finite element model. A finer mesh was then applied to the geometry until there was no significant change (grid independent solution) in the pressure distribution inside the short-tube. This process resulted in a mesh size of 3885 elements needed for the model: 2010 for the fluid domain and 1875 for the structural domain. This mesh size was used for all calculations.

To run the program, an initial, undeformed shape of the short-tube was assumed along with a pressure distribution. The initial pressure distribution was that for a rigid short-tube operating at the same upstream and downstream pressures. Fig. 3 shows the pressure profiles after each successive iteration of the numerical model. The profiles showed no change after the fourth iteration. Iterations in the model were coupled. First, the non-linear fluid equations were solved,
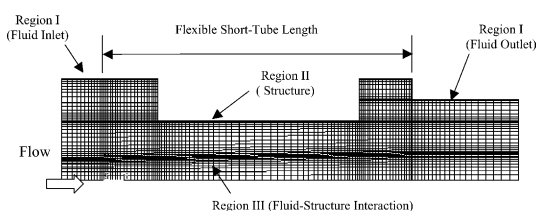
Fig. 2. Axisymmetric computational domain for the flexible short-tube orifice.
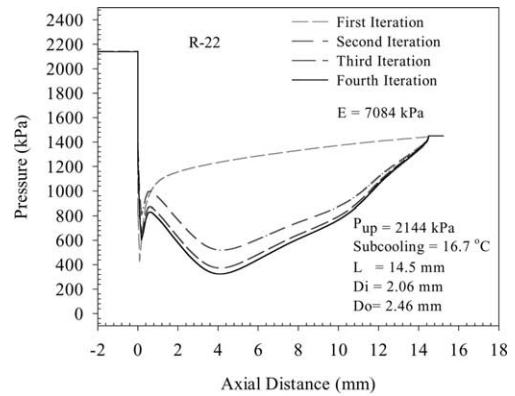
Fig. 3. Pressure profile change for R-22 single-phase flow through a flexible short-tube at successive iterations for a modulus of elasticity of 7084 kPa.

which provided a pressure distribution estimate inside the short-tube. This pressure distribution was then transferred as an internal area boundary condition to the solids model which was used to solve for the tube deformation. The deformation was then used to specify the new flow boundary in the flow model. The pressure and flow were then recalculated in the flow model. The resulting estimate of the pressure field inside the short-tube was again used to recalculate the deformation in the solid model. This process was repeated until there was no change in the pressure profile or shape. The profile corresponding to the first iteration in this figure represents the initial guess for the internal pressure distribution along the non-deformed tube.

4. Results and discussions

The estimated pressure profiles for three moduli of elasticity (5313, 7084 and 9889 kPa) as well as for the undeformed tube at two upstream pressures (1179 and 2144 kPa) are shown in Figs. 4 and 5, respectively. The 7084 and 9889 kPa were moduli for which experimental data were available [4]. The 5513 kPa would represent the most flexible short-tube of the three. The upstream pressure of 1179 kPa corresponds to a saturation temperature of almost 30 °C while 2144 kPa corresponds to a saturation temperature of 54 °C.

Both Figs. 4 and 5 show that the lowest modulus (5513 kPa) tube yielded the lowest pressures inside the short-tube for both upstream pressures. The figures also show two distinctive pressure drop regions for flexible short-tubes. A sharp pressure drop occurred at the tube inlet due to the rapid acceleration of the fluid as a result of the sudden change in the cross-section, which was followed by a pressure recovery. This sharp drop at the inlet was due to the vena-contracta. The most rigid tube (9889 kPa) produced a higher pressure drop at the tube
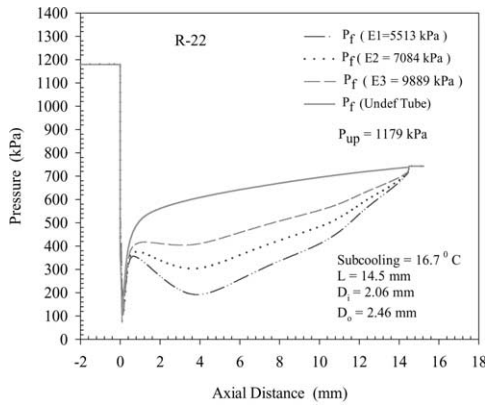
NORMAL

Fig. 4. Pressure profiles for R-22 single-phase flow through a flexible short-tube for three moduli of elasticity with an upstream pressure of 1179 kPa.
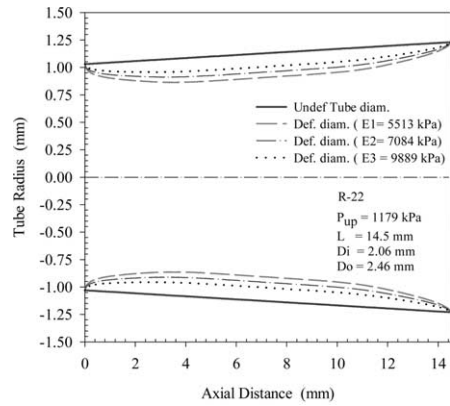

Fig. 6. Effect of the modulus of elasticity on short-tube diameter ratio for upstream pressures ranging from 1179 to 2144 kPa.
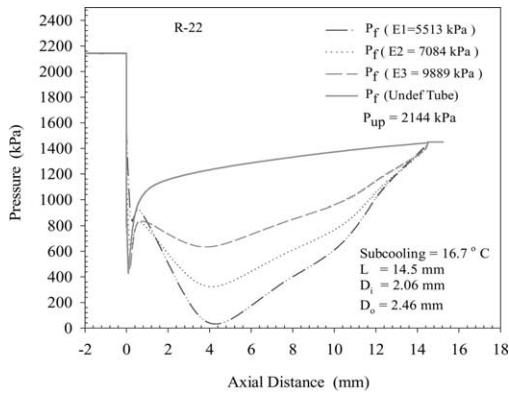

Fig. 5. Pressure profiles for R-22 single-phase flow through a flexible short-tube for three moduli of elasticity and an upstream pressure of 2144 kPa.
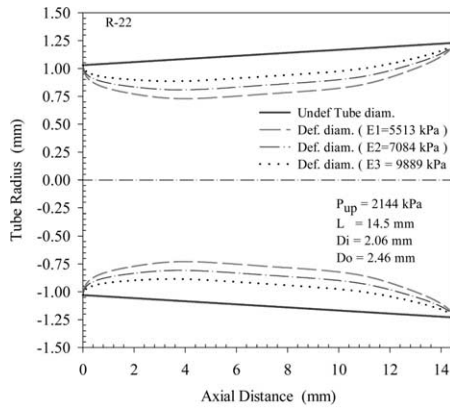

Fig. 7. Radius variation along the axis of a short-tube with R-22 single-phase flow for three moduli of elasticity and an upstream pressure of 1179 kPa.

inlet than the most flexible one (5513 kPa). The pressure profiles for a rigid short-tube in Figs. 4 and 5 are for comparison purposes to show how the expected profile in the flexible short-tube is different. The rigid short-tube had the largest pressure drop at the vena-contracta. This phenomena can be attributed to the lack of deformation at the tube inlet for the rigid short-tube.

As the modulus of elasticity decreases, the tube gets more flexible and, hence, the inlet edge buckles more upon tube deformation. The large buckling near the tube inlet produces a chamfering-like effect which decreases the vena-contracta effect near the inlet of the short-tube. Therefore, a smaller dip in pressure was estimated at the inlet for the more flexible short-tube.

The second pressure drop shown in Figs. 4 and 5 is caused by the deformation of the flexible short-tube. Figs. 6 and 7 show the internal shape of the deformed tube for two upstream pressures (1179 and 2144 kPa, respectively). Both figures display the tube internal diameter variation upon deformation for three different

moduli of elasticity (5513, 7084, 9889 kPa). Further, the figures show the tube's gradual variation from the original non-deformed shape to the most deformed shape corresponding to the more flexible tube (5513 kPa).

For both upstream pressures, the figures show that the deformed shape estimated by the model resembled a converging-diverging nozzle. The tube had a chamfered-like rounded inlet and outlet as a result of the deformation caused by the pressure difference between external and internal pressures. A visible increase in the chamfering-like inlet angle was observed as the modulus of elasticity decreased (flexibility increased). The figures show that there was a measurable change in the short-tube new internal shape for the three moduli of elasticity at the two studied pressures. The minimum tube cross-section area occurred at an axial distance approximately 3.0–4.5 mm from the short-tube inlet. This location corresponded to the second pressure dip shown in Figs. 4 and 5. The deformed shape helps explain the estimated pressure profiles inside the tube. As the flow approached

the tube inlet, a sharp pressure drop occurred due to the sudden reduction in area. This drop was higher for the highest modulus tube due to the inlet effect.

The diameter ratio is defined as the deformed average diameter along the tube to the non- deformed average diameter along the tube. This ratio was introduced to better quantify the tube deformation for different material properties and under different applied loads. Therefore, it was plotted as a function of the modulus of elasticity and upstream pressure as illustrated in Fig. 6. In Fig. 8, for all upstream pressures there was a change of the slope when the modulus of elasticity decreased beyond approximately 6800 kPa (960 psi). This indicated that under the same load, the more flexible the tube, the more sensitive response to the applied loads, and, accordingly, the higher the reduction in the tube cross-sectional area. For stiffer materials, the diameter ratio continued to increase and would converge to unity for rigid tubes. Referring to the new axial radius distribution shown in Figs. 7 and 8, the average increase of diameter ratio as the modulus of elasticity increased ranged from 5 to 13% as the upstream pressure varied from 1179 to 2144 kPa. Thus, a short-tube with a lower modulus of elasticity will have a smaller diameter ratio for the same upstream pressure. The lower diameter ratio also implies a smaller deformed diameter and smaller flow rate.

The flexible short-tube was designed to better control the refrigerant flow rate when the operating conditions in the condenser change. Fig. 9 shows the predicted mass flow rate versus modulus of elasticity at different upstream (condenser) pressures. The general trend of the curves was that mass flow rate decreased as tube flexibility increased (modulus of elasticity decreases). The authors in [4] reported that the slope of the mass flow rate through the flexible short-tube changed as a function of the modulus of elasticity of the short-tube material.

As the modulus of elasticity decreased below 6500 kPa, the curves approached each other and showed a rapid decrease in mass flow rate. Thus, reducing the modulus of elasticity of the short-tube material may lead to an excessive contraction of the tube under higher upstream pressures, which may overly restrict refrigerant flow. Hence, there might be a critical value for the tube modulus of elasticity under which the mass flow rate might sharply and undesirably decrease.

As the modulus of elasticity (the tube gets stiffer) increased, the flow appeared to approach an asymptotic value for the smaller upstream pressures. For example, at an upstream pressure of 1179 kPa, the mass flow rate began to level out as the modulus of elasticity reached values greater than approximately 8000 kPa. This would indicate that the stiffer materials provide sufficient resistance at this upstream pressure that there is relatively little change in the shape of the short-tube. Fig. 9 shows that the slope of the mass flow curves increased as the upstream pressures increased for a modulus of elasticity greater than 8000 kPa. It would appear that the higher upstream pressures provide enough force to deform even the stiffer materials studied here.

The local pressure everywhere along the tube was lower for the higher upstream pressure compared to the lower pressure (Fig. 10). Downstream of the recovery region inside the short-tube, a pressure drop was observed at axial distances from 3.5 to 4.5 mm from the front edge of the short-tube. The higher the upstream pressure, the more observable the dip at the same axial location. This may be attributed to more stress on the tube material as a result of increasing the upstream pressure which led the tube to constrict more than at the lower upstream pressure. For all upstream pressures, the pressure distribution inside the tube increased downstream of the dip as a result of the diverging shape of the tube inner area over the last 10 mm of the tube.
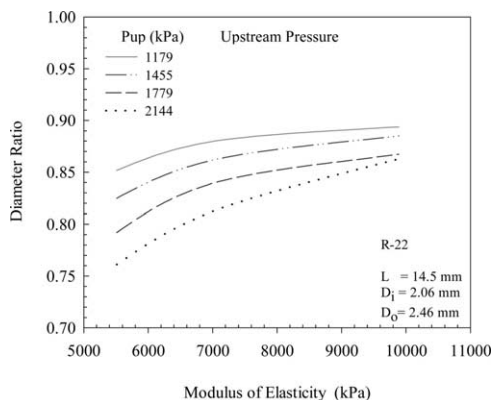

Fig. 8. Radius variation along the axis of a short-tube with R-22 single-phase flow for three moduli of elasticity and an upstream pressure of 2144 kPa.
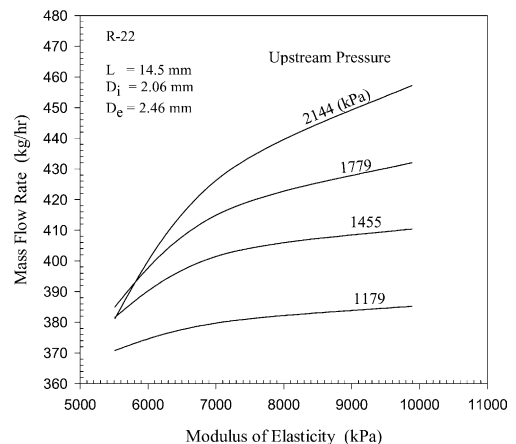

Fig. 9. Mass flow rate variation with short-tube modulus of elasticity for R-22 single-phase flow.
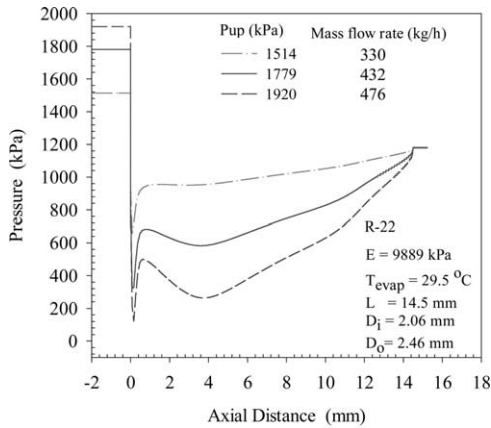
Fig. 10. Pressure profiles for R-22 single-phase flow through a flexible short-tube for upstream pressures ranging from 1514 to 1920 kPa.
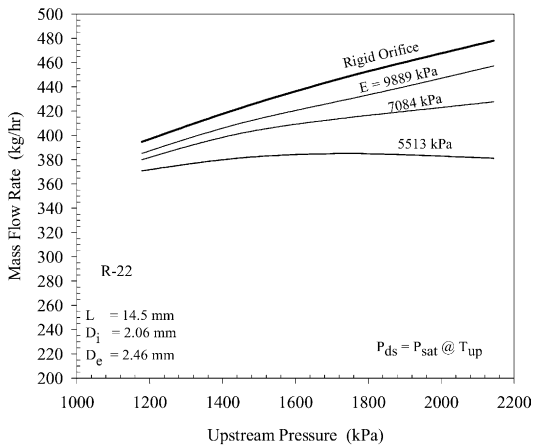

Fig. 11. Mass flow versus upstream pressure for R-22 single-phase flow through a flexible short-tube for three moduli of elasticity.

The mass flow rate through short-tubes was dependent on the upstream pressure. Fig. 11 shows the variation of mass flow rate through the short-tube as a function of the upstream pressure for different moduli of elasticity. The mass flow rate increased as the upstream pressure increased. Fig. 11 illustrates that the slope of the mass flow rate changed as a function of the tube modulus of elasticity. This was also observed in the experimental data collected by the authors in [4].

As the modulus of elasticity decreased, the tube flexibility increased and, hence, the tube contracted more as upstream pressure increased. This concept can be seen in the figure for the lower modulus short-tube that produced a mass flow rate that averaged 10% lower than the higher modulus short-tube (9889 kPa). In [4], it was concluded that, based on experimental data, this average percentage was 6% for the two moduli (7084 and 9889 kPa). For the same moduli, this percentage was
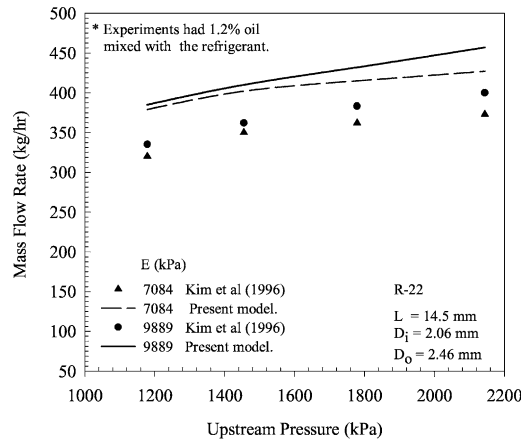

Fig. 12. Mass flow rate comparison between numerical and experimental results for single-phase flow of R-22 through a flexible short-tube.

4% for the numerical results. Fig. 11 illustrates that as the upstream pressure increased, the mass flow rate increased for the higher modulus of elasticity tubes. However, as the tube became more flexible (lower modulus of elasticity), there was a tendency for the flow rate to decrease as the upstream pressure increased beyond a certain value. For a very flexible tube, the higher exerted force produced by the higher upstream pressure created a large enough deformation to severely restrict the flow.

A comparison of the numerical results with some available published experimental data is shown in Fig. 12. The figure illustrates that the trends were similar for both the experimental data and the results from the computational model. As the upstream pressure increased, the mass flow rate increased for a single-phase flow as shown in this figure. Furthermore, shown in Fig. 12 is the close agreement between numerical and experimental results as the slope of the trend changed for the lower modulus tube at an upstream pressure more than 1400 kPa. Quantitatively, the numerical model over-predicted the mass flow rate. The computed numerical results were 14% higher than the experimental data. One possible reason for the differences between the model and the experimental data is that the data were for a mixture of 1.2% mineral oil and refrigerant, while the model results were for pure R-22. The addition of oil can have a measurable effect on the mass flow through short-tubes [14].

5. Conclusions

The finite element model produced physically realistic results as long as the tube deformation was not too large. As the tube elasticity increased and/or the applied pressure load was increased excessively, the model showed unrealistic pressure distributions which might

indicate the collapse of the tube. The model provided visualization of the pressure distribution and tube deformation that would be difficult to measure experimentally because of the size of the flexible short-tube geometry. Although the numerical model had the limitation of handling only single-phase flow, it predicted reasonable flow rates compared to published experimental results.

When deformed, the tube shape resembled a converging-diverging nozzle. The tube had a chamfered-like inlet and outlet as a result of deformation caused by upstream pressure. A significant increase (almost from 3 to 8) in the chamfering-like inlet angle was observed as the modulus of elasticity decreased. The lower the modulus of elasticity, the less pressure drop at the tube inlet due to the chamfered-like inlet after deformation, and the higher pressure drop along the tube due to the higher tube contraction.

As the modulus of elasticity decreased, the mass flow rate decreased for all upstream pressures and it approached each other beyond a certain value of modulus of elasticity. Similarly, as the upstream pressure increased, the mass flow rate increased for all moduli of elasticity; however, the lower modulus tube exhibited a lower flow rate that tended to decrease as the upstream pressure increased. The study showed that the more flexible tube restricted the mass flow rate by 2–6% less than the less flexible tube depending on the upstream pressure.

References

[1] Drucker AS. Variable area refrigerant expansion device having a flexible orifice. US Patent 5134860, 1992.

[2] Drucker AS, Abbott AD. Variable area refrigerant expansion device having a flexible orifice. US Patent 5214939, 1993.

[3] Drucker AS, Cann PL. Variable area refrigerant expansion device having a flexible orifice. US Patent 5031416, 1991.

[4] Kim YC, O'Neal DL, Payne WV, Farzad M. Refrigerant flow through flexible short-tube orifices. Int J HVAC&R Research 2002;8(2):179–90.

[5] Mei VC. Short-tube refrigerant restrictors. ASHRAE Trans 1982;88(2):157–68.

[6] Krakow KI, Lin S. Refrigerant flow through orifices. ASHRAE Trans 1988;94(1):484–506.

[7] Aaron AA, Domanski PA. Experimentation, analysis, and correlation of refrigerant-22 flow through short-tube restrictors. ASHRAE Trans 1990;96(1):729–42.

[8] Kuehl SJ, Goldschmidt VW. Flow of R-22 through short-tube restrictors. ASHRAE Trans 1992;98(2):59–64.

[9] Kim Y. Two-phase flow of HCFC-22 and HFC-134a through short-tube orifices. PhD dissertation, Texas A&M University, College Station, TX, USA, 1993.

[10] Kim Y, O'Neal DL. Two-phase flow of R-22 through short-tube orifices. ASHRAE Trans 1994;100(1):323–34.

[11] Kim Y, O'Neal DL. A semi-empirical model of two-phase flow of refrigerant-134a through short-tube orifices. Experimental Thermal and Fluid Science 1994;9(4):426–35.

[12] Erbay HA, Demiray H. Finite axisymmetric deformations of elastic tubes: an approximation method. J Engng Math 1995;29:451–72.

[13] Swanson Analysis System Inc. Theory, vol IV, ANSYS user's manual. Houston, PA, USA: Swanson Analysis System Inc; 1995.

[14] Kim Y, O'Neal D. The effect of oil on the two-phase critical flow of refrigerant 134a through short-tube orifices. International Journal of Heat and Mass Transfer 1994; 37(9):1377–86.